Coherent perfect absorption in epsilon-near-zero metamaterials

Simin Feng* and Klaus Halterman

Michelson Lab, Physics Division, Naval Air Warfare Center, China Lake, California 93555, USA

(Received 10 April 2012; revised manuscript received 17 September 2012; published 2 October 2012)

In conventional materials, strong absorption usually requires that the material have either high loss or a large thickness-to-wavelength ratio ($d/\lambda \gg 1$). We find the situation to be vastly different for bilayer structures composed of a metallic substrate and an anisotropic epsilon-near-zero (ENZ) metamaterial, where the permittivity in the direction perpendicular to its surface, ϵ_z, vanishes. Remarkably, perfect absorption can occur in situations where the metamaterial is arbitrarily thin ($d/\lambda \ll 1$) and arbitrarily low loss. Our numerical and analytical solutions reveal that under the conditions $\epsilon_z \to 0$ and $\Im(\epsilon_z) \gg \Re(\epsilon_z)$, at perfect absorption there is a linear relationship between the thickness and the loss, which means the thickness of the absorber can be pushed to zero by reducing the material loss to zero. This counterintuitive behavior is explained in terms of coherent perfect absorption (or stimulated absorption) via critical coupling to a fast wave propagating along the ENZ layer.

DOI: 10.1103/PhysRevB.86.165103 PACS number(s): 41.20.Jb, 41.90.+e, 78.67.Pt

I. INTRODUCTION

Many exotic phenomena have been predicted for metamaterials[1–3] by tuning the permittivity ϵ and permeability μ. One of the unique metamaterials, coined ϵ-near-zero (ENZ), or some of the high-impedance[4] metamaterials, of which the permittivity is made vanishingly small, has attracted considerable attention due to many unusual phenomena.[5–10] Slabs of ENZ metamaterials can give rise to enhanced magnification and absorption under certain circumstances.[11] In ENZ media loss can induce transparency, omnidirectional collimation, and anti–Snell's law refraction.[12] Anisotropic loss can even improve propagation of oblique incident beams.[12]

Strong absorption typically requires either high loss or large thickness. Total absorption in a shallow grating was discovered a long time ago.[13] With the development of metamaterials, there is a renewed interest in perfect absorption (PA). Although perfect absorption has been demonstrated in various ultrathin patterned surfaces,[14–32] the physical explanations for enhanced absorption are unsatisfactory, since perfect absorption can occur in the homogenization limit[32] where there is no scattering element to couple light into the media. The common feature in those absorbers can be described by a bilayer model composed of a high-impedance absorbing layer on a reflective substrate. Recent publications indicate that the thickness-to-wavelength ratio in this type of structure can be continuously reduced. What is the limit? How small can this ratio be? To answer these questions, in this paper we investigate perfect absorption of p-polarized waves in a bilayer consisting of an ENZ material on a metal, as shown in Fig. 1. The ENZ region has a uniform surface without scattering elements. The metallic layer can be either a perfect electric conductor (PEC) or real metal which is thick enough to ensure no transmission. Interestingly, we find that when the material loss approaches zero, the ratio of the ENZ thickness to wavelength must go to zero as well to ensure perfect absorption. To verify this counterintuitive phenomenon, we derive an analytical formula which shows a linear relationship between the thickness and the loss. This absorption anomaly *cannot* be explained by the Fabry-Pérot effect or by leaky mode excitation. Thanks to the recent theory of coherent perfect absorption,[33,34] we will show that the exotic phenomenon can be explained by coherent perfect absorption which couples light to a fast wave propagating along the ENZ medium.

II. THEORETICAL APPROACH

Our investigation is based on an anisotropic ENZ ($\epsilon_{1x} = 1$, $\epsilon_{1z} \approx 0$) material as shown in Fig. 1. For simplicity, the plane of incidence is assumed to be coincident with one of the crystal planes. In the following, the subscripts 1 and 2 refer, respectively, to the ENZ medium and metal. The areas above the ENZ and below the metal are free space and refer to regions 0 and 3, respectively. Since the ϵ_{1x} has no significant impact, unless stated otherwise, $\epsilon_{1x} = 1$ is assumed throughout the paper. First we show that an above-light-line surface plasmon polariton (SPP) can arise at the interface between the ENZ metamaterial and metal. This unique feature assists perfect coupling of light to the structure. The propagation constant of SPP at the interface of two semi-infinite anisotropic media is given by

$$\frac{k_{\rm spp}}{k_0} = \sqrt{\frac{\epsilon_{1z}\epsilon_{2z}(\epsilon_{2x}\mu_{1y} - \epsilon_{1x}\mu_{2y})}{\epsilon_{2x}\epsilon_{2z} - \epsilon_{1x}\epsilon_{1z}}} \approx \sqrt{\epsilon_{1z}\mu_{1y}(1-\delta)}, \quad (1)$$

where $k_0 = \omega/c$ and $\delta = \epsilon_{1x}\mu_{2y}/(\epsilon_{2x}\mu_{1y})$. The approximation is due to the fact that $\epsilon_1 \ll |\epsilon_2|$. In our case, $\mu_{1y} = \mu_{2y} = 1$ and $\epsilon_{2x} = \epsilon_{2z} = \epsilon_m \sim -10^5$ (in the IR region). Thus, $k_{\rm spp}/k_0 \approx \sqrt{\epsilon_{1z}\mu_{1y}} < 1$, which characterizes above-light-line SPP dispersion, and is clearly different from conventional SPP dispersion.

Assuming a harmonic time dependence $\exp(-i\omega t)$ for the EM field, from Maxwell's equations we have

$$\begin{aligned} \nabla \times \left(\bar{\bar{\mu}}_n^{-1} \cdot \nabla \times \boldsymbol{E}\right) &= k_0^2(\bar{\bar{\epsilon}}_n \cdot \boldsymbol{E}), \\ \nabla \times \left(\bar{\bar{\epsilon}}_n^{-1} \cdot \nabla \times \boldsymbol{H}\right) &= k_0^2(\bar{\bar{\mu}}_n \cdot \boldsymbol{H}), \end{aligned} \quad (2)$$

where $\bar{\bar{\epsilon}}_n$ and $\bar{\bar{\mu}}_n$ are, respectively, the permittivity and permeability tensors for a given (uniform) region ($n = 0,1,2,\ldots$), which in the principal coordinates are described by

$$\begin{aligned} \bar{\bar{\epsilon}}_n &= \epsilon_{nx}\hat{\boldsymbol{x}}\hat{\boldsymbol{x}} + \epsilon_{ny}\hat{\boldsymbol{y}}\hat{\boldsymbol{y}} + \epsilon_{nz}\hat{\boldsymbol{z}}\hat{\boldsymbol{z}}, \\ \bar{\bar{\mu}}_n &= \mu_{nx}\hat{\boldsymbol{x}}\hat{\boldsymbol{x}} + \mu_{ny}\hat{\boldsymbol{y}}\hat{\boldsymbol{y}} + \mu_{nz}\hat{\boldsymbol{z}}\hat{\boldsymbol{z}}. \end{aligned} \quad (3)$$

We consider TM modes, corresponding to nonzero field components H_y, E_x, and E_z. The magnetic field H_y satisfies

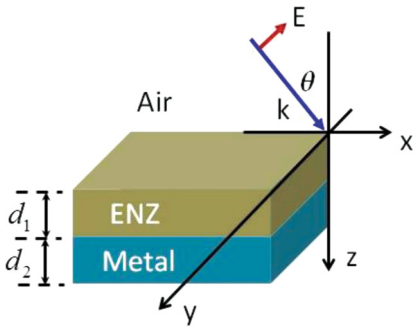

FIG. 1. (Color online) A plane wave is incident (at an angle θ) on an anisotropic ($\epsilon_{1x} = 1$ and $\epsilon_{1z} \approx 0$) ENZ/metal bilayer with thicknesses d_1 and d_2 for the ENZ medium and metal (Ag), respectively. The substrate layer can be either real metal or PEC.

the following wave equation:

$$\frac{1}{\epsilon_z}\frac{\partial^2 H_y}{\partial x^2} + \frac{1}{\epsilon_x}\frac{\partial^2 H_y}{\partial z^2} + k_0^2 \mu_y H_y = 0, \tag{4}$$

which admits solutions of the form $\psi(z)\exp(i\beta x)$. The parallel wave vector β is determined by the incident wave, and is conserved across the interface,

$$\beta^2 = k_0^2 \epsilon_{nz}\mu_{ny} - \alpha_n^2 \frac{\epsilon_{nz}}{\epsilon_{nx}}, \quad (n = 0,1,2,\ldots), \tag{5}$$

where α_n is the wave number in the z direction. The functional form of $\psi(z)$ is either a simple exponential $\exp(i\alpha_n z)$ for the semi-infinite region or a superposition of $\cos(\alpha_n z)$ and $\sin(\alpha_n z)$ terms for the bounded region (along the z direction). The other two components E_x and E_z can be found by solving Maxwell's equations.

For a better understanding, in the following the absorption anomaly is investigated for both PEC and silver substrates. For perfect absorption, the substrate should be as reflective as a PEC. However, for comparison we include analysis for a real metal substrate. Thus, PA here is not in the strictest mathematical sense, but rather in a practical sense, meaning effectively 100%. The permittivity of silver in the infrared region is obtained by curve-fitting experimental data[35] with a Drude model, $\epsilon_m = 1 - \omega_p^2/\omega^2$, where the "plasma frequency" $\omega_p = 6.02\ \mu\text{m}^{-1}$. In the case of silver substrate, it is an open boundary and the electromagnetic fields were computed numerically based on the scattering matrix method by matching boundary conditions at each interface, i.e., continuity of H_y and E_x. The transmittance (T) and reflectance (R) were calculated via the Poynting vector $\boldsymbol{S}$, given by $\boldsymbol{S} = c/8\pi\Re(\boldsymbol{E} \times \boldsymbol{H}^*)$. From energy conservation the absorptance (A) is given by $A = 1 - T - R$. Since the transmittance of the ENZ-Ag bilayer is effectively zero ($T \sim 10^{-10}$; see bottom panels in Fig. 2), PA occurs when the reflectance is zero (see top panels in Fig. 2), where the angular dependent effective impedance ($\mathcal{Z}_{em}$) of the ENZ-Ag structure matches that of free space ($\mathcal{Z}_0$); i.e., $\mathcal{Z}_{em} = \mathcal{Z}_0$. The effective impedance of the ENZ Ag can be derived as

$$\mathcal{Z}_{em} \equiv \mathcal{Z}_1 \frac{1 - r_{12}\exp(i2\phi)}{1 + r_{12}\exp(i2\phi)} = \mathcal{Z}_0, \tag{6}$$

where $r_{12} = (\mathcal{Z}_1 - \mathcal{Z}_2)/(\mathcal{Z}_1 + \mathcal{Z}_2)$, $\mathcal{Z}_j = \alpha_j/\epsilon_{jx}$ $(j = 0,1,2)$, and $\phi = \alpha_1 d_1$. Equation (6) determines the perfect absorption

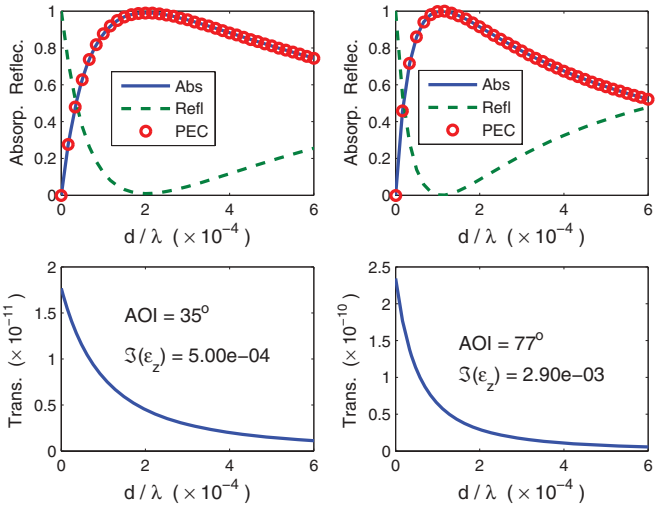

FIG. 2. (Color online) Absorptance and reflectance (top panels), as well as transmittance (bottom panels) vs the d/λ at the AOI = 35° (left panels) and AOI = 77° (right panels) when the substrate is Ag. The thickness of the Ag-layer $d_2 = 200$ nm. The permittivity of Ag is taken at $\lambda = 100\ \mu$m. The transmittance of the ENZ-Ag is near zero ($\sim 10^{-10}$). In the top panels, the absorptance (blue solid) and reflectance (green dashed) clearly satisfy the relation $A = 1 - R$. Perfect absorption occurs at the zero reflection when $d/\lambda = 2 \times 10^{-4}$ and $\Im(\epsilon_z) = 5 \times 10^{-4}$ (left panels), and when $d/\lambda = 1 \times 10^{-4}$ and $\Im(\epsilon_z) = 2.9 \times 10^{-3}$ (right panels). $\Re(\epsilon_z) = 10^{-4}$. The red circles represent the absorptance of the ENZ-PEC structure, agreeing very well with that of the ENZ-Ag bilayer (blue solid).

angle which also corresponds to the effective Brewster angle since the reflection is zero and occurs only for p-polarized waves at oblique incidences.

In the case of a PEC substrate, there is no transmission and the electric field $E_x = 0$ at the ENZ-PEC interface. Thus, the magnetic field H_y takes the form $\cos[\alpha_1(z - d_1)]$ when the origin of the $\hat{z}$ coordinate is located at the air-ENZ interface. By matching boundary conditions at the air-ENZ interface, it is straightforward to derive the reflection coefficient of the magnetic field as

$$r = \frac{1 + \eta\tan\phi}{1 - \eta\tan\phi}, \tag{7}$$

where $\eta = i\,\mathcal{Z}_1/\mathcal{Z}_0$. The reflected electric field $E_x = \mathcal{Z}_0 H_y$. From the Poynting vector, the reflectance of the EM power is $R = |r|^2$; thus the absorptance $A = 1 - R$. Perfect absorption corresponds to a zero reflection coefficient where the effective impedance ($\mathcal{Z}_{ep}$) of the ENZ-PEC structure is matched to that of free space. From Eq. (7), we thus have

$$\mathcal{Z}_{ep} \equiv -i\,\mathcal{Z}_1 \tan\phi = \mathcal{Z}_0. \tag{8}$$

In the PEC limit $(\mathcal{Z}_2 \to 0)$, Eq. (6) reduces to Eq. (8). Both Eqs. (6) and (8) indicate that perfect absorption depends on the angle of incidence (AOI), permittivity, and ratio of ENZ thickness to wavelength. The tangent of the angle (θ_S) that the Poynting vector inside the ENZ makes at the air-ENZ interface is given by

$$\tan\theta_S = \frac{\Re(S_x)}{\Re(S_z)} = \frac{\beta/k_0}{\Re(\epsilon_{1x})\,\Re[-i\,\mathcal{Z}_1\tan\phi]}. \tag{9}$$

So, the Poynting angle is a function of thickness ($\phi = \alpha_1 d_1$). If incident from air, $\beta/k_0 = \sin\theta$ and $\mathcal{Z}_0 = \cos\theta$. Substituting Eq. (8) into the above, we obtained the following relationship between the perfect absorption angle (θ_P) and the angle (θ_S) at the air-ENZ interface:

$$\tan\theta_P = \epsilon_{1x}\tan\theta_S, \tag{10}$$

where ϵ_{1x} is real. Although both θ_P and θ_S depend on the ENZ thickness, they satisfy a simple relationship.

III. DISCUSSION

In the following figures and discussion, the subscript 1 for the ENZ medium will be omitted without ambiguity. Figure 2 shows the absorptance, reflectance, and transmittance versus the ratio of ENZ thickness to wavelength (d/λ) for the ENZ-Ag bilayer at two different AOI. For comparison, in the top panels the absorptance of the ENZ-PEC structure is presented in the red circles which was calculated from Eq. (7) via $A = 1 - |r|^2$. The PEC result agrees very well with that of numerical simulation for the Ag substrate based on our scattering matrix method. Here perfect absorption occurs at the extremely small loss and thickness-to-wavelength ratio. Potentially, this effect can significantly reduce the thickness of absorbers in the radio frequency (RF) region. For example, when the wavelength $\lambda = 1$ m, the ratio $d/\lambda = 0.0001$ will result in $d = 100$ μm, which is achievable with the current metamaterial fabrication technology.

We find that perfect absorption always occurs at oblique incidence. More interestingly, for a fixed AOI, a smaller dissipation $\Im(\epsilon_z)$ *requires* a smaller d/λ ratio to achieve perfect absorption, as shown in the right panels of Fig. 3, where the absorptance is plotted in a 2D domain of d/λ and $\Im(\epsilon_z)$ at two fixed AOI for a PEC substrate. The color scheme indicates that there is a linear relationship between the ratio d/λ and dissipation $\Im(\epsilon_z)$ for PA to occur. To analyze this anomaly, we resort to the reflection coefficient of the ENZ-PEC bilayer. When $d \ll \lambda$, $\epsilon_z \to 0$, and $\Re(\epsilon_z) \ll \Im(\epsilon_z)$, from Eq. (8) we obtain the following relationship:

$$\frac{d}{\lambda} = \frac{\Im(\epsilon_z)}{2\pi\sin\theta\tan\theta}. \tag{11}$$

The above equation shows a linear relationship between the d/λ and $\Im(\epsilon_z)$ and explains the peculiar behavior in Fig. 3. For any AOI, when $\Im(\epsilon_z) \to 0$, the ratio d/λ must go to zero as well to ensure perfect absorption. Equation (11) provides a guidance for reducing the thickness of absorbers. To verify Eq. (11), the left panels of Fig. 3 show the perfect absorption trajectory, d/λ vs $\Im(\epsilon_z)$, which is obtained from both numerical (blue solid) and analytical (green circles) methods, showing consistency. Due to the anisotropic nature, the propagation phase in the $\hat{z}$ direction inside the ENZ medium is not zero. Clearly, Eq. (11) indicates that perfect absorption cannot be explained by the Fabry-Pérot effect since there is no standing wave. The perfect absorption angle (θ_P) can be derived from Eq. (11):

$$\cos\theta_P = -\sigma + \sqrt{1+\sigma^2}, \quad \sigma \equiv \frac{\Im(\epsilon_z)}{2k_0 d}. \tag{12}$$

Thus, $\theta_P \to 0^\circ$ when $\sigma \to 0$, and $\theta_P \to 90^\circ$ when $\sigma \to \infty$.

Figure 4 shows the absorptance as a function of AOI and d/λ for the PEC (right top) and Ag (right bottom) substrates, along with the corresponding perfect absorption angle (left panels) as a function of d/λ. For comparison, each perfect absorption angle is calculated with two methods. The blue-solid curves are numerically extracted from the 2D absorptance corresponding to the right panels. The green

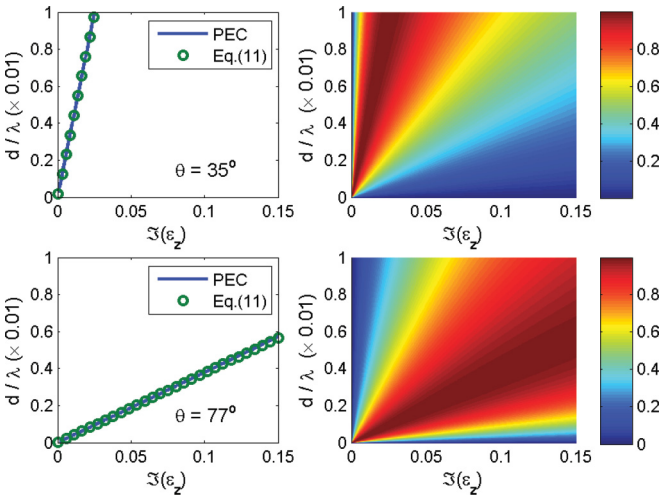

FIG. 3. (Color online) Right panels: Absorptance as a function of $\Im(\epsilon_z)$ and d/λ at the AOI $= 35^\circ$ (top) and AOI $= 77^\circ$ (bottom) for the ENZ-PEC bilayer. $\Re(\epsilon_z) = 10^{-4}$. Color bars represent the magnitude of the absorptance. The dark-red region indicates the odd behavior that the lower loss requires thinner material to achieve PA. Left panels: PA trajectory, d/λ vs $\Im(\epsilon_z)$, which is extracted numerically (blue solid) from the absorptance corresponding to the right panel and is calculated analytically (green circles) from Eq. (11). Similar phenomenon is also observed for the Ag substrate (not shown).

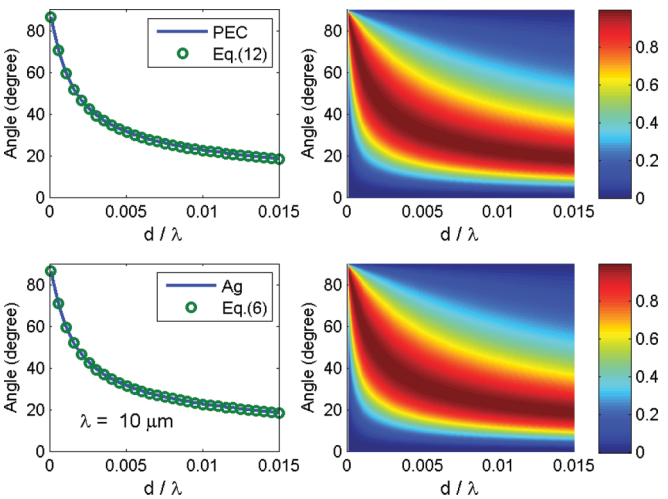

FIG. 4. (Color online) Right panels: Absorptance vs AOI and d/λ for the PEC (top) and Ag (bottom) substrates. $\epsilon_z = 0.001 + 0.01i$. The thickness of the Ag-layer $d_2 = 200$ nm. The permittivity of Ag is taken at $\lambda = 10$ μm. Left panels: Perfect absorption angle vs d/λ. The perfect absorption angles were numerically extracted (blue solid) from the absorptance corresponding to the right panel. For comparison, the green circles represent the PA angles calculated from Eq. (12) for the PEC substrate and computed from Eq. (6) for the Ag substrate.

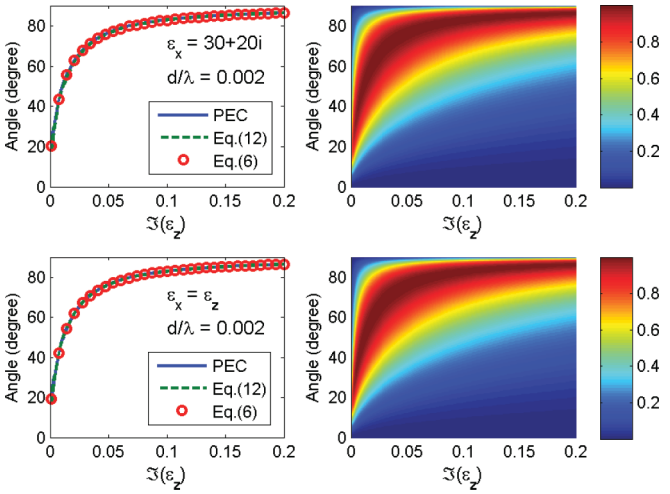

FIG. 5. (Color online) Right panels: Absorptance vs AOI and $\Im(\epsilon_z)$ for ENZ-PEC bilayer when $\epsilon_x = 30 + 20i$ (top panels) and $\epsilon_x = \epsilon_z$ (bottom panels, isotropic ENZ). $\Re(\epsilon_z) = 0.001$ and $d/\lambda = 0.002$. Left panels: Perfect absorption angle vs $\Im(\epsilon_z)$ numerically extracted (blue solid) from the absorptance corresponding to the right panels, analytically calculated (green dashed) from Eq. (12), and numerically computed (red circles) from impedance matching Eq. (6) where the permittivity of Ag was taken at the $\lambda = 10\ \mu$m.

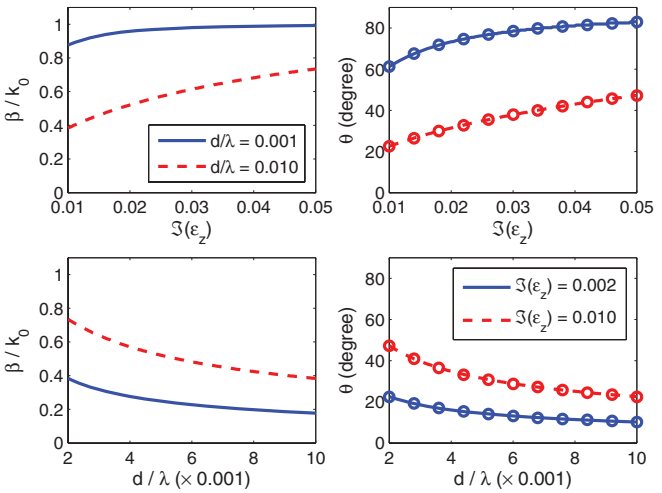

FIG. 6. (Color online) CPA zeros. Propagation constant β/k_0 vs $\Im(\epsilon_z)$ (left top) and d/λ (left bottom). Right panels represent the corresponding angles calculated from $\sin^{-1}(\beta/k_0)$. The circles are the PA angles numerically extracted from 2D absorptance. In the top panels, $d/\lambda = 0.001$ (blue-solid curves) and $d/\lambda = 0.01$ (red-dashed curves). In the bottom panels, $\Im(\epsilon_z) = 0.002$ (blue-solid curves) and $\Im(\epsilon_z) = 0.01$ (red-dashed curves). $\Re(\epsilon_z) = 0.0001$.

circles are calculated from Eq. (12) for the PEC substrate and from the impedance matching condition Eq. (6) for the Ag substrate. Clearly, regarding power transport, PEC is a satisfactory model of silver in the far-infrared region. Notice that as $d/\lambda \to 0$, $\theta_P \to 90^\circ$, and thus $\theta_S \to 90^\circ$ [see Eq. (10)], which means the power flow inside the ENZ medium is parallel to the surface. In fact, when $d/\lambda \ll 1$, as shown later, the ENZ-metal bilayer structures can support fast waves $\left[\Re(\beta) < k_0 \text{ and } \Im(\beta) = 0\right]$ which propagate along the ENZ layer and provide a new mechanism for absorption. Figure 5 shows the 2D absorptance of the ENZ-PEC bilayer as a function of AOI and $\Im(\epsilon_z)$ (right panels) for different ϵ_x values, as well as the corresponding perfect absorption angle vs $\Im(\epsilon_z)$ (left panels). It is evident that ϵ_x does not have much influence on the absorption when $d/\lambda \ll 1$. To show consistency, in the left panels the perfect absorption angle is calculated from three different methods including the one for the Ag substrate (red circles) computed from the impedance matching [Eq. (6)]. The three methods are all consistent and thus further validate Eqs. (11) and (12). When realistic materials parameters are considered, dispersion near the ENZ frequency cannot be avoided. Although perfect absorption occurs only at the single frequency, high absorption in a range centered at the ENZ frequency can still be possible with bandwidth depending on how smoothly the permittivity crosses zero. Lately, an idea of realizing broadband ENZ materials has been proposed.[36,37] Alternative plasmonic materials with real permittivity varying smoothly across zero have also been fabricated.[38,39] These progresses show a promising future for potential ENZ applications.

IV. COHERENT PERFECT ABSORPTION

Figures 2–5 confirm the anomalous perfect absorption in the ENZ/metal bilayer structures. Particularly, Eqs. (11) and (12) provide a concise analytical expression to describe this exotic behavior. Physically, how could this be possible as both dissipation and thickness approach zero, yet perfect absorption can still occur? This phenomenon can be explained by coherent perfect absorption (or stimulated absorption).[33] Coherent perfect absorption (CPA) is a time-reversed process of lasing at threshold[33] and a perfect mode conversion mechanism.[34] The CPA zeros can be solved from Eq. (8) by searching for a real propagation constant, i.e., $\Im(\beta) = 0$. These results are shown in the left panels of Fig. 6. The right panels of Fig. 6 represent the corresponding angles converted from the CPA zeros via $\sin^{-1}(\beta/k_0)$. To verify that these angles are indeed the perfect absorption angles, we simulated 2D absorptance and numerically extracted the PA angles from the simulation. The numerical results are presented by the circles in the right panels of Fig. 6. The correlations found in the above results demonstrate a clear consistency with the CPA mechanism. In fact, Eq. (11) describes the critical coupling condition, i.e., the specific amount of dissipation required to achieve PA.[33] The CPA zeros are distinct from leaky modes which, as the name indicated, have a leaky character, i.e., $\Im(\beta) \neq 0$. A leaky mode cannot be excited by a plane wave incident on a uniform surface without scattering elements, whereas CPA occurs at the perfect match of the incident field with that of the CPA zeros. Under the condition $d/\lambda \ll 1$, the ENZ-metal bilayer supports fast waves propagating parallel to the interface. These modes extend into free space and naturally match to plane waves as shown in Fig. 7, which demonstrates the spatial distribution of the energy density of the fast wave in different regions when perfect absorption occurs. The energy density (U) can be obtained from [8]

$$U = \frac{1}{16\pi}\Re\left[\boldsymbol{E}^\dagger \cdot \frac{\partial(\omega\bar{\bar{\epsilon}})}{\partial\omega}\boldsymbol{E} + \boldsymbol{H}^\dagger \cdot \frac{\partial(\omega\bar{\bar{\mu}})}{\partial\omega}\boldsymbol{H}\right]. \quad (13)$$

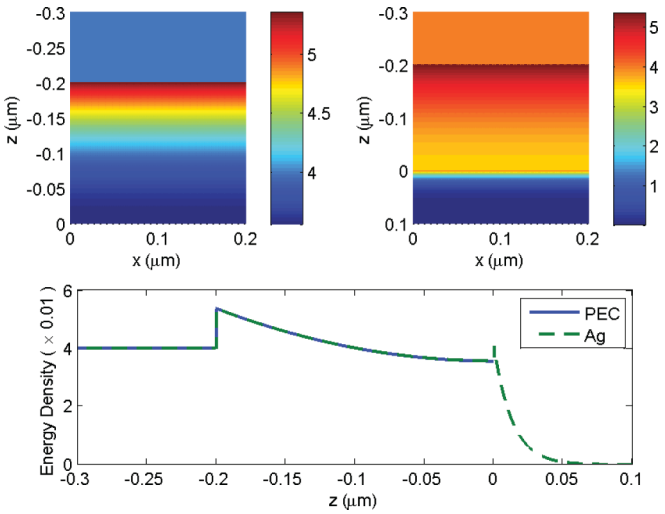

FIG. 7. (Color online) Spatial distribution of energy density (normalized so that H_y is unity at the ENZ-air interface) at the AOI = 16° for the ENZ-PEC (top left) and ENZ-Ag (top right) structures. The ENZ layer with thickness 0.2 μm is located at $z \in [-0.2,0]$. The region $z \in [-0.3,-0.2]$ is air. In the top-left panel, the PEC has zero thickness. In the top-right panel, the region $z \in [0,0.1]$ is silver. The permittivity of Ag is taken at $\lambda = 10$ μm. Color bars represent the magnitude ($\times 0.01$) of the energy density. $\epsilon_z = 0.001 + 0.01i$. Bottom panel: A comparison of the energy density distribution in the ENZ-PEC (blue solid) and ENZ-Ag (green dashed) bilayers.

In our case, the frequency-dependent permittivity in Eq. (13) is applied to the silver substrate since the Drude model was used as mentioned earlier in the main text. For comparison, the top-left panel in Fig. 7 shows the result from the ENZ-PEC structure, while the top-right panel is for the ENZ-Ag bilayer. In the top-right panel, a thin-layer above-light-line SPP (since $\epsilon_z \ll 1$) is evidently excited at the ENZ-Ag interface and the field outside the Ag layer is near zero. The strong field at the ENZ-air interface is distinguishable from conventional surface waves, since in this case the exponential decay of the field occurs strictly inside the ENZ medium. Outside of the ENZ, the field neither decays like a surface wave nor does it increase like a leaky wave. The observed uniformity indicates that the field outside the structure is a plane wave matching with the free-space wave, and thus can be excited by a plane wave incidence—a striking difference from surface waves and leaky waves. Figure 7 shows perfect match of the plane wave with the fast wave of $\Im(\beta) = 0$ at the critical coupling. With the precise amount of dissipation which is a function of d/λ and AOI [see Eq. (11)], light can be effectively coupled to a fast wave via CPA which, as a mode converter,[34] perfectly transfers the incident power into a surface current. Since both transmission and reflection are effectively zero, for the nearly lossless and near-zero thickness ENZ, propagation along the layer becomes the only channel for the EM power to flow. The reflective substrate provides a feedback; otherwise a second input field is needed to achieve this phenomenon.[33] The consistent results between the real metal substrate and the PEC substrate (see Figs. 2–5 and Fig. 7) indicate that the light is mostly absorbed in the ENZ layer.

V. SUMMARY

In summary, we have demonstrated perfect absorption in ENZ-metal structures when both material loss and thickness approach zero simultaneously. The linear relationship between loss and thickness suggests the idea of using material loss to control thickness to achieve ultrathin absorbers. This unconventional phenomenon can be understood in terms of coherent perfect absorption. This viewpoint provides a different perspective and a deep insight on high-impedance meta-absorbers and may impact future absorber designs, as well as lasing materials. Although our explanation is based on ENZ-metal bilayers, we believe the CPA mechanism is quite representative for various ultrathin deep subwavelength patterns on a reflective surface. ENZ materials have been realized in high-impedance surfaces,[4,15–19] as well as in nanowire arrays[40,41] and nanolayers.[42] Ultrathin absorption can be beneficial for radar-absorbing materials. Narrow-band perfect absorption at the specific angle has potential applications in notch filters and directional absorbers for highly sensitive target identifications of biological and chemical agents.

ACKNOWLEDGMENTS

S. Feng acknowledges the sponsorship of NAVAIR's Core S&T EO Initiative and ILIR programs.

*Corresponding author: simin.feng@navy.mil

[1] J. B. Pendry, D. Schurig, and D. R. Smith, Science **312**, 1780 (2006).
[2] S. Feng and K. Halterman, Phys. Rev. Lett. **100**, 063901 (2008).
[3] Y. Lai, H. Chen, Z.-Q. Zhang, and C. T. Chan, Phys. Rev. Lett. **102**, 093901 (2009).
[4] D. Sievenpiper, L. Zhang, R. F. J. Broas, N. G. Alexópolous, and E. Yablonovitch, IEEE Trans. Microwave Theory Tech. **47**, 2059 (1999).
[5] S. Enoch, G. Tayeb, P. Sabouroux, N. Guérin, and P. Vincent, Phys. Rev. Lett. **89**, 213902 (2002).
[6] M. Silveirinha and N. Engheta, Phys. Rev. Lett. **97**, 157403 (2006).
[7] V. C. Nguyen, L. Chen, and K. Halterman, Phys. Rev. Lett. **105**, 233908 (2010).
[8] K. Halterman, S. Feng, and V. C. Nguyen, Phys. Rev. B **84**, 075162 (2011).
[9] A. Alù, M. G. Silveirinha, A. Salandrino, and N. Engheta, Phys. Rev. B **75**, 155410 (2007).
[10] D. C. Adams, S. Inampudi, T. Ribaudo, D. Slocum, S. Vangala, N. A. Kuhta, W. D. Goodhue, V. A. Podolskiy, and D. Wasserman, Phys. Rev. Lett. **107**, 133901 (2011).
[11] Y. Jin, S. Xiao, N. A. Mortensen, and S. He, Opt. Express **19**, 11114 (2011).
[12] S. Feng, Phys. Rev. Lett. **108**, 193904 (2012).
[13] M. C. Hutley and D. Maystre, Opt. Commun. **19**, 431 (1976).
[14] N. Engheta, *IEEE Antennas and Propagation Society International Symposium*, Vol. 2 (IEEE, New York, 2002), pp. 392–395.

[15]N. I. Landy, S. Sajuyigbe, J. J. Mock, D. R. Smith, and W. J. Padilla, Phys. Rev. Lett. **100**, 207402 (2008).
[16]X. Liu, T. Starr, A. F. Starr, and W. J. Padilla, Phys. Rev. Lett. **104**, 207403 (2010).
[17]H. Li, L. H. Yuan, B. Zhou, X. P. Shen, Q. Cheng, and T. J. Cuia, J. Appl. Phys. **110**, 014909 (2011).
[18]F. Costa, A. Monorchio, and G. Manara, IEEE Trans. Antennas Propag. **58**, 1551 (2010).
[19]J. R. Brown, A. P. Hibbins, M. J. Lockyear, C. R. Lawrence, and J. R. Sambles, J. Appl. Phys. **104**, 043105 (2008).
[20]Y. Avitzour, Y. A. Urzhumov, and G. Shvets, Phys. Rev. B **79**, 045131 (2009).
[21]Y. Q. Ye, Y. Jin, and S. He, J. Opt. Soc. Am. B **27**, 498 (2010).
[22]V. G. Kravets, F. Schedin, and A. N. Grigorenko, Phys. Rev. B **78**, 205405 (2008).
[23]N. Liu, M. Mesch, T. Weiss, M. Hentschel, and H. Giessen, Nano Lett. **10**, 2342 (2010).
[24]G. Kang, I. Vartiainen, B. Bai, and J. Turunen, Opt. Express **19**, 770 (2011).
[25]R.-L. Chern and W.-T. Hong, Opt. Express **19**, 8962 (2011).
[26]A. Yanai, M. Orenstein, and U. Levy, Opt. Express **20**, 3693 (2012).
[27]C. Wu and G. Shvets, Opt. Lett. **37**, 308 (2012).
[28]J. Le Perchec, P. Quémerais, A. Barbara, and T. López-Ríos, Phys. Rev. Lett. **100**, 066408 (2008).
[29]K. Aydin, V. E. Ferry, R. M. Briggs, and H. A. Atwater, Nature Commun. **2**, 517 (2011).
[30]N. Bonod, G. Tayeb, D. Maystre, S. Enoch, and E. Popov, Opt. Express **16**, 15431 (2008).
[31]E. Popov, D. Maystre, R. C. McPhedran, M. Nevière, M. C. Hutley, and G. H. Derrick, Opt. Express **16**, 6146 (2008).
[32]E. Popov, S. Enoch, and N. Bonod, Opt. Express **17**, 6770 (2009).
[33]Y. D. Chong, L. Ge, H. Cao, and A. D. Stone, Phys. Rev. Lett. **105**, 053901 (2010).
[34]H. Noh, Y. Chong, A. D. Stone, and H. Cao, Phys. Rev. Lett. **108**, 186805 (2012).
[35]E. D. Palik, *Handbook of Optical Constants of Solids* (Academic Press, San Diego, 1998).
[36]L. Sun and K. W. Yu, J. Opt. Soc. Am. B **29**, 984 (2012).
[37]L. Sun and K. W. Yu, Appl. Phys. Lett. **100**, 261903 (2012).
[38]G. V. Naik, J. Kim, and A. Boltasseva, Opt. Mater. Express **1**, 1090 (2011).
[39]G. V. Naik, J. L. Schroeder, X. Ni, A. V. Kildishev, T. D. Sands, and A. Boltasseva, Opt. Mater. Express **2**, 478 (2012).
[40]R. J. Pollard, A. Murphy, W. R. Hendren, P. R. Evans, R. Atkinson, G. A. Wurtz, A. V. Zayats, and V. A. Podolskiy, Phys. Rev. Lett. **102**, 127405 (2009).
[41]L. V. Alekseyev, E. E. Narimanov, T. Tumkur, H. Li, Yu. A. Barnakov, and M. A. Noginov, Appl. Phys. Lett. **97**, 131107 (2010).
[42]M. J. Roberts, S. Feng, M. Moran, and L. Johnson, J. Nanophoton. **4**, 043511 (2010).